Solid-State NMR Determination of $^{13}C\alpha$ Chemical Shift Anisotropies for the Identification of Protein Secondary Structure

Mei Hong

Contribution from the Department of Chemistry, Iowa State University, Ames, Iowa 50011

Received November 24, 1999. Revised Manuscript Received February 22, 2000

Abstract: A solid-state nuclear magnetic resonance (NMR) method for the site-resolved identification of the secondary structure of solid peptides and proteins is presented. This technique exploits the correlation between the backbone conformation and the Cα chemical shift anisotropies (CSA) of proteins. The $^{13}C\alpha$ CSAs are measured under fast magic-angle-spinning using a new sequence of sixteen 180° pulses with special timing to reintroduce the CSA interaction selectively. Quantitative values of the shielding anisotropies are determined from the magnetization decay, as demonstrated for several amino acids. To achieve high-resolution spectra, this CSA filter experiment is combined with 2D $^{15}N-^{13}C$ correlation spectroscopy. Applied to selectively and extensively ^{13}C-labeled and uniformly ^{15}N-labeled ubiquitin at the largest dephasing time, the 2D experiment yields a spectral pattern that corresponds primarily to α-helical residues. This agrees with the previous finding that helical residues have smaller CSAs than sheet residues. However, the quantitative CSA differences between the helical and sheet conformations are less pronounced than indicated by solution-state NMR. This CSA filter technique provides an efficient and site-resolved method for characterizing the secondary structure of extensively isotopically labeled proteins.

Introduction

The structure determination of proteins that cannot be crystallized or tumble slowly in solution is a challenging problem in biochemistry. Most membrane proteins and fibrous proteins belong to this category, and have not been amenable to study by single-crystal X-ray diffraction or liquid-state nuclear magnetic resonance (NMR) spectroscopy. Solid-state NMR is the spectroscopic tool of choice for characterizing the structure of disordered and amorphous solids in detail, because it does not require long-range order or rapid isotropic molecular tumbling. To determine the secondary structure of these solid peptides and proteins, several solid-state NMR experiments that measure the backbone torsion angles ϕ and ψ have been developed.[1−9] One of these techniques has also been combined with selective and extensive biosynthetic isotopic labeling to determine multiple ϕ torsion angles in a model protein, ubiquitin.[7] Although these torsion-angle methods can provide accurate information on the protein backbone conformation, their successful implementation requires reproducible spectral intensities, which calls for extensive signal averaging. Thus, additional robust methods for determining and refining the protein secondary structure are desirable.

The NMR chemical shift interaction is a useful probe of the conformation of protein backbones. The chemical shift results from the shielding of the external magnetic field by the electrons surrounding the nucleus. The orientation dependence of this interaction is manifested through the chemical shift anisotropy (CSA). Because of the electronic nature of the chemical shielding, both the isotropic and anisotropic chemical shielding correlate with chemical bonding. In addition, the chemical shielding depends on molecular conformation. An example is the γ-gauche effect in long aliphatic chains, where a gauche conformation around the bond next nearest to the nucleus of interest shifts the isotropic frequency upfield by about 5 ppm compared to the trans conformation.[10,11] In peptides and proteins, the Cα isotropic chemical shifts exhibit downfield displacements of about +3 ppm in the helical conformation compared to the random coil structure, while the β-sheet conformation displays upfield shifts of about −1 ppm.[12] Such conformation-induced, secondary**,** isotropic chemical shifts have been widely used as indicators of the protein secondary structure.[13,14] Clearly, changes in the isotropic chemical shifts must originate from changes in the chemical shielding values along the three principal axes of the chemical shift tensor. These changes will likely affect the breadth of the chemical shift tensor. Indeed, Tjandra and Bax observed that the shielding spans of Cα correlate with the protein secondary structure.[15] By measuring the interference between the $^{13}C\alpha$ CSA and the $^{13}C-^{1}H$ dipolar

(1) Schmidt-Rohr, K. *Macromolecules* **1996**, *29*, 3975−3981.
(2) Weliky, D.; Tycko, R. *J. Am. Chem. Soc.* **1996**, *118*, 8487−8488.
(3) Feng, X.; Eden, M.; Brinkmann, A.; Luthman, H.; Eriksson, L.; Graslund, A.; Antzutkin, O. N.; Levitt, M. H. *J. Am. Chem. Soc.* **1997**, *119*, 12006−12007.
(4) Hong, M.; Gross, J. D.; Griffin, R. G. *J. Phys. Chem. B* **1997**, *101*, 5869−5874.
(5) Costa, P. R.; Gross, J. D.; Hong, M.; Griffin, R. G. *Chem. Phys. Lett.* **1997**, *280*, 95−103.
(6) Hong, M.; Gross, J. D.; Hu, W.; Griffin, R. G. *J. Magn. Reson.* **1998**, *135*, 169−177.
(7) Hong, M. *J. Magn. Reson.* **1999**, *139*, 389−401.
(8) Feng, X.; Verdegem, P. J. E.; Lee, Y. K.; Sandstrom, D.; Eden, M.; Bovee-Geurts, P.; Grip, W. J. d.; Lugtenburg, J.; Groot, H. J. M. d.; Levitt, M. H. *J. Am. Chem. Soc.* **1997**, *119*, 6853−6857.
(9) Gregory, D. M.; Mehta, M. A.; Shields, J. C.; Drobny, G. P. *J. Chem. Phys.* **1997**, *107*, 28−42.
(10) Schmidt-Rohr, K.; Spiess, H. W. *Multidimensional solid-state NMR and Polymers*; Academic Press: San Diego, 1994.
(11) Tonelli, A. E. *J. Am. Chem. Soc.* **1980**, *102*, 7635−7637.
(12) Spera, S.; Bax, A. *J. Am. Chem. Soc.* **1991**, *113*, 5490−5492.
(13) Wishart, D. S.; Sykes, B. D. *J. Biomol. NMR* **1994**, *4*, 171−180.
(14) Wishart, D. S.; Sykes, B. D.; Richards, F. M. *Biochemistry* **1992**, *31*, 1647−1651.
(15) Tjandra, N.; Bax, A. *J. Am. Chem. Soc.* **1997**, *119*, 9576−9577.

10.1021/ja994119n CCC: $19.00
Published on Web 03/30/2000

relaxation mechanisms in solution, they found the Cα shielding anisotropies of helical residues to be significantly smaller than those of sheet residues. Meanwhile, Oldfield and co-workers carried out ab initio calculations on the individual components of the Cα and Cβ shielding tensors in a number of β-substituted amino acids.[16] Their calculations confirmed that the Cα CSAs depend on the backbone geometry in the same fashion as observed by solution NMR, but with a smaller CSA difference between the helical and sheet conformations.[17]

Solid-state NMR is the most direct method for measuring anisotropic frequencies, since the orientation dependence of the nuclear spin interactions is not averaged by the overall reorientation of the molecules. Although various techniques for CSA determination exist, none presents the high resolution and sensitivity required for application to proteins. For example, a slow magic-angle spinning (MAS) technique has been used to determine the principal elements of the Cα shielding tensor to correlate with the backbone torsion angles.[17] However, this experiment has low resolution and sensitivity due to the need for MAS sidebands in the spectra. Other CSA measuring techniques require nonstandard probes that change the spinner orientations during each scan; additionally, during the time required for rotor-axis reorientation, spin diffusion can occur, which interferes with the correlation between the anisotropic and the isotropic chemical shifts.[18−22] A robust CSA measuring technique for proteins must be applicable under fast magic-angle spinning to achieve the necessary sensitivity and site resolution.

In this paper, we introduce a technique for determining the chemical shift anisotropies of Cα sites in proteins with high resolution. With a simple one-dimensional pulse sequence suitable under fast MAS, the experiment preferentially destroys the magnetization of spins with larger CSAs while retaining that with smaller CSAs. We demonstrate on amino acids that this "CSA filter" yields quantitative values of the breadth of the chemical shielding tensor. To obtain high resolution for proteins, we combine this CSA measurement with two-dimensional (2D) $^{15}N-^{13}C$ correlation. The 2D-resolved CSA filter is demonstrated on the 76-residue protein ubiquitin, which yields a spectral pattern that corresponds well to the α-helical residues. Importantly, by identifying secondary structure motifs through the absence (β-sheet) or presence (α-helix) of peaks in the 2D spectra, the experiment complements the precise determination of backbone torsion angles by the tensor correlation approach. Given suitable site resolution and resonance assignment, this α-helix selection approach has the potential of permitting a rapid diagnosis of the protein secondary structure for many residues simultaneously. Finally, we compare the CSA values extracted from the solid-state CSA-filter experiment with the solution NMR results and with the ab initio calculations.

Experimental Section

^{13}C-Labeled Amino Acids. A model compound designated A/G/L was prepared by mixing approximately equal weights of [3-^{13}C]alanine, [2-^{13}C]glycine, and [1-^{13}C]leucine (Cambridge Isotope Lab). The amino acid mixture is a good compound for testing the CSA filter experiment, since it allows three different CSA parameters to be measured simultaneously.

^{13}C,^{15}N-Labeled Ubiquitin. Selectively and extensively ^{13}C-labeled and uniformly ^{15}N-labeled ubiquitin were overexpressed by VLI-Research (Malvern, PA). Cells were grown in M9 minimal media whose sole carbon source was [2-^{13}C]glycerol and whose sole nitrogen source was ^{15}N-ammonium sulfate. The selective and extensive ^{13}C-labeling approach was designed to enrich specific carbons at high levels while not labeling others.[7] By keeping the labels relatively isolated, we minimize line broadening in the spectra. The labeled sites originating from [2-^{13}C]glycerol have been determined previously.[7] In particular, eighteen out of twenty amino acids are labeled at the ^{13}Cα position. Nine of these ^{13}Cα labels have no direct ^{13}C neighbors, thus simplifying the spin dynamics. About 25 mg of the protein powder was packed into a 4-mm rotor and hydrated to 30% (w/w) in water. Hydration reduces the conformational heterogeneity of the sample, thereby improving the spectral resolution.

Solid-State NMR. The NMR experiments were carried out at the University of Massachusetts on a Bruker DSX-300 spectrometer operating at a Larmor frequency of 75.5 MHz for ^{13}C and 300.13 MHz for ^{1}H. A triple-resonance MAS probe equipped with a 4-mm probehead was used. Typical spinning speeds were 7000 ± 2 Hz, regulated by a MAS controller. Proton decoupling fields of about 120 kHz were used. Carbon 90° and 180° pulse lengths were about 3.5 and 7 μs, while ^{15}N pulse lengths were about 5.5 and 11 μs. Ramped cross polarization with variable ^{13}C radiofrequency fields was used to maximize polarization transfer.[23]

The resonances in the 2D $^{15}N-^{13}C$ spectra were assigned based on the solution NMR chemical shifts.[24] The solid-state isotropic chemical shifts have recently been shown by 2D and 3D MAS correlation experiments to be very similar to the solution state values.[25,26] The crystal structure of ubiquitin[27] was used to assign the secondary structure to the individual residues. With these two pieces of information, we correlated the shielding anisotropies with the secondary structure motifs.

The CSA decay curves were simulated using a Fortran program as described before.[6] Briefly, the MAS time signals were numerically calculated based on eqs 2 and 3 below. The τ values were incremented from 0 to 1 rotor period (τ_r) at equal intervals. Powder averaging was carried out in 3° steps for the Euler angles α and β, and 6° steps for γ. The input parameters were the three principal values of the chemical shift tensor, the duration of the π-pulse train for $\tau = 0$, the number of τ steps, and the spinning speed. The chemical shift principal values were input in frequency units, using a Larmor frequency of 75.5 MHz, which corresponds to the experimental magnetic field strength. All CSA decay curves are presented in terms of the shielding span $\Delta\sigma = \sigma_{33} - \sigma_{11}$, which is related to the anisotropy parameter δ by $\Delta\sigma = \delta(3 + \eta)/2$. The asymmetry parameter η is defined as $\eta = (\sigma_{22} - \sigma_{11})/(\sigma_{33} - \sigma_{iso})$. Since the isotropic chemical shift is averaged to zero by the pulse sequence, the three input principal values were constrained to have a sum of zero, i.e., $\sigma_{iso} = \sigma_{11} + \sigma_{22} + \sigma_{33} = 0$. The calculated time signals were transferred to MATLAB and compared with the experimental decay curves. The root-mean-square deviation (rmsd) between the experiment and the simulation were calculated in MATLAB as

$$\mathrm{rmsd}(\Delta\sigma,\eta) = [\sum_{i=1}^{n}(S_{expt} - S_{calc}(\Delta\sigma,\eta,\tau_i))^2/n]^{1/2} \qquad (1)$$

Here n represents the number of data points measured or calculated in each CSA decay curve. The rmsd is parametrically dependent on η, which affects the CSA decay as discussed below.

(16) Havlin, R. H.; Le, H.; Laws, D. D.; deDios, A. C.; Oldfield, E. *J. Am. Chem. Soc.* **1997**, *119*, 11951−11958.
(17) Heller, J.; Laws, D. D.; Tomaselli, M.; King, D. S.; Wemmer, D. E.; Pines, A.; Havelin, R. H.; Oldfield, E. *J. Am. Chem. Soc.* **1997**, *119*, 7827−7831.
(18) Gan, Z. H. *J. Am. Chem. Soc.* **1992**, *114*, 8307.
(19) Hughes, C. D.; Sherwood, M. H.; Alderman, D. W.; Grant, D. M. *J. Magn. Reson.* **1993**, *102*, 58−72.
(20) Bax, A.; Szeverenyi, N. M.; Maciel, G. E. *J. Magn. Reson.* **1983**, *55*, 494−497.
(21) Terao, T.; Fujii, T.; Onodera, T.; Saika, A. *Chem. Phys. Lett.* **1984**, *107*, 145−148.
(22) Frydman, L.; Chingas, G. C.; Lee, Y. K.; Grandinetti, P. J.; Eastman, M. A.; Barrall, G. A.; Pines, A. *J. Chem. Phys.* **1992**, *97*, 4800.
(23) Metz, G.; Wu, X.; Smith, S. O. *J. Magn. Reson. Ser. A* **1994**, *110*, 219−227.
(24) Wang, A. C.; Bax, A. *J. Am. Chem. Soc.* **1996**, *118*, 2483−2494.
(25) Hong, M. *J. Biomol. NMR* **1999**, *15*, 1−14.
(26) Straus, S. K.; Bremi, T.; Ernst, R. R. *J. Biomol. NMR* **1998**, *12*, 39−50.
(27) Vijay-Kumar, S.; Bugg, C. E.; Cook, W. J. *J. Mol. Biol.* **1987**, *194*, 531−544.

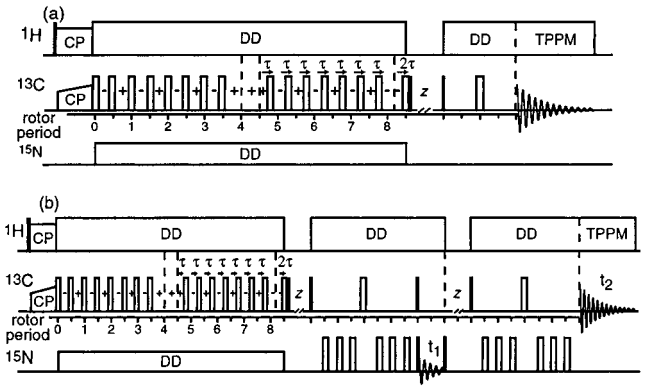

Figure 1. Pulse sequences for the CSA-filter experiment. (a) 1D: The CSA-filter pulse train consists of sixteen 180° pulses phase-cycled by the xy-16 scheme. The pulses are spaced at half a rotor period apart, except for additional displacements between the eighth and ninth pulses, and between the fifteenth and sixteenth pulse. A z-filter for obtaining purely absorptive cosine-modulated signals and a Hahn echo are applied before detection. Filled rectangles: 90° pulses. Open rectangles: 180° pulses. The plus and minus signs represent the sign of the dynamic phases under the chemical shift evolution. (b) 2D $^{15}N-^{13}C$ correlated CSA filter: The ^{15}N chemical shift evolution is inserted between the 180°-pulse train and the ^{13}C detection period. REDOR is used to transfer the coherence between ^{15}N and ^{13}C.

Theory of Chemical Shift Anisotropy Recoupling. The pulse sequence for the 1D CSA-filter experiment is shown in Figure 1a. After cross polarization (CP) from ^1H to ^{13}C, a train of sixteen 180° (π) pulses is applied on the ^{13}C channel. The phases of these pulses follow the xy-16 scheme[28] to minimize the effects of pulse and phase imperfections. The 180° pulses are applied in synchrony with magic-angle spinning with the following timing. The first eight pulses occur at an interval of half a rotor period, beginning with the first 180° pulse immediately after CP. At the end of the eighth pulse, one rotor period is allowed to elapse without any pulse. An additional variable delay τ is then added before the ninth 180° pulse is applied. Thus, the ninth pulse occurs at $t = 4.5\tau_r + \tau$ after CP. The next six pulses are again spaced at half a rotor period apart, so that they occur at time τ after either the end or the middle of a rotor period. The last, sixteenth, pulse is spaced by $0.5\tau_r + \tau$ from the fifteenth pulse and thus occurs at $t = 8\tau_r + 2\tau$ after CP.

Throughout the π-pulse train, a continuous pulse is applied on the ^{15}N channel to remove the $^{13}C-^{15}N$ dipolar interaction. Following the 180° ^{13}C pulses, a z-filter, consisting of two 90° pulses separated by a period without ^1H decoupling, is applied on the ^{13}C channel. The phase of the first 90° pulse is orthogonal to the ^{13}C spin lock phase to select the cosine component of the magnetization. Finally, the ^{13}C signal is detected after a Hahn echo.

The π-pulse train with the above specific timing is designed to yield an average Hamiltonian of pure anisotropic chemical shift, without the isotropic chemical shift or the $^{13}C-^{15}N$ dipolar interaction. The net evolution under the isotropic chemical shift is zero because the total lengths of intervals corresponding to positive and negative isotropic frequencies are equal. Since the isotropic chemical shift is independent of molecular orientations, the different rotor orientations at the beginning of each interval do not affect the evolution of the magnetization. In contrast, the anisotropic chemical shift depends on the orientation of the rotor. The shielding anisotropy would only be refocused if no variable delay τ is inserted so that the second half of the pulse train would begin precisely at $t = 4.5\tau_r$. In that case, the positions of the second eight pulses would exactly match those of the first eight pulses. By inserting a variable delay τ to displace the second eight pulses with respect to the first eight pulses, the CSA interaction is not completely refocused. The phase acquired during the evolution under the CSA depends on τ, the anisotropy δ (or $\Delta\sigma$), and the number of rotor periods, n, corresponding to the first half of the π-pulse train. The larger the δ, the faster the magnetization decays. The number of rotor periods can be any integer multiple of 4. The longer the pulse train, the faster the CSA decay with τ.

The time-dependent anisotropic chemical shift frequency $\omega(t)$ under MAS is written as

$$\omega(t) = \delta\left[\frac{C_1}{\delta}\cos(\gamma + \omega_r t) + \frac{C_2}{\delta}\cos(2\gamma + 2\omega_r t) + \frac{S_1}{\delta}\sin(\gamma + \omega_r t) + \frac{S_2}{\delta}\sin(2\gamma + 2\omega_r t)\right] \quad (2)$$

where the coefficients C_1, C_2, S_1, and S_2 depend on δ, η, and the Euler angles (α, β, γ) that describe the relative orientation of the principal axis frame of the chemical shift tensor with respect to a rotor-fixed frame.[10,29] Due to the sign reversal induced by the successive 180° pulses at the specified positions of the pulse sequence, the accumulated phase of the magnetization $\Phi(t) = \int_0^t \omega(t')\,dt'$ is

$$\begin{aligned}
\Phi_{CSA}(\tau) &= [-\int_0^{\tau_r/2}\omega(t)\,dt + \int_{\tau_r/2}^{\tau_r}\omega(t)\,dt]*n + [\int_\tau^{\tau_r/2+\tau}\omega(t)\,dt - \int_{\tau_r/2+\tau}^{\tau}\omega(t)\,dt]*n + \int_0^\tau\omega(t)\,dt - \int_\tau^{2\tau}\omega(t)\,dt \\
&= -2\int_0^{\tau_r/2}\omega(t)\,dt*n + 2\int_\tau^{\tau_r/2+\tau}\omega(t)\,dt*n + \int_0^\tau\omega(t)\,dt - \int_\tau^{2\tau}\omega(t)\,dt \\
&= -2n\int_0^{\tau_r/2}\omega(t)\,dt + 2n\int_\tau^{\tau_r/2+\tau}\omega(t)\,dt + \int_0^\tau\omega(t)\,dt - \int_\tau^{2\tau}\omega(t)\,dt \\
&= -2n\int_0^{\tau}\omega(t)\,dt + 2n\int_{\tau_r/2}^{\tau}\omega(t)\,dt + 2n\int_\tau^{\tau_r/2+\tau}\omega(t)\,dt + \int_0^\tau\omega(t)\,dt - \int_\tau^{2\tau}\omega(t)\,dt \\
&= -(2n-1)\int_0^{\tau}\omega(t)\,dt + 2n\int_{\tau_r/2}^{\tau_r/2+\tau}\omega(t)\,dt - \int_\tau^{2\tau}\omega(t)\,dt
\end{aligned} \quad (3)$$

Equation 3 indicates that the magnetization acquires a finite CSA phase at $\tau \neq n\tau_r$ ($n = 0, 1, 2, ...$) that is periodic with the rotation period τ_r. When $\tau = \tau_r/2$, the CSA phase is particularly simple:

$$\begin{aligned}
\Phi_{CSA}\left(\frac{\tau_r}{2}\right) &= -(2n-1)\int_0^{\tau_r/2}\omega(t)\,dt + 2n\int_{\tau_r/2}^{\tau_r}\omega(t)\,dt - \int_{\tau_r/2}^{\tau_r}\omega(t)\,dt \\
&= -(2n-1)\int_0^{\tau_r/2}\omega(t)\,dt + (2n-1)\int_{\tau_r/2}^{\tau_r}\omega(t)\,dt \\
&= -(4n-2)\int_0^{\tau_r/2}\omega(t)\,dt
\end{aligned} \quad (4)$$

The detected signals are modulated by $\cos(\Phi_{CSA}(\tau,\delta,\eta))$. Thus, by monitoring the signal intensities as a function of τ, we can determine the magnitude of δ or $\Delta\sigma$. The minimum number of τ values needed to determine the CSA is three: $\tau = 0$ provides the reference spectrum to which the intensities at larger τ values are normalized, and two more data points are required since both $|\delta|$ and η are unknown. In practice, it is advantageous to acquire more than three τ data points, so that $|\delta|$ or $|\Delta\sigma|$ can be determined more precisely based on the redundancy of the information encoded in the intensities at multiple τ values. In the limit of short filter times τ, the CSA phase in eq 3 is directly proportional to the anisotropy δ, since

$$\Phi_{CSA}(\tau\rightarrow 0) = -(2n-1)\cdot\omega(0)\tau + 2n\cdot\omega(\tau_r/2)\tau - \omega(t_r/2)\tau \propto \delta\cdot\tau \quad (5)$$

Therefore, the cosine-modulated signals,

(28) Gullion, T.; Baker, D. B.; Conradi, M. S. *J. Magn. Reson.* **1990**, *89*, 479−484.

(29) Maricq, M. M.; Waugh, J. S. *J. Chem. Phys.* **1979**, *70*, 3300−3316.

$$\cos(\Phi_{CSA}(\tau \rightarrow 0)) \propto \cos(\delta\tau) \approx 1 - (\delta\tau)^2/2 \quad (6)$$

decrease quadratically with increasing $|\delta|$ at small τ values. This proves that the magnetization of sites with larger CSAs exhibits a faster initial decay.

In principle, the shielding anisotropy can be measured by an alternative pulse sequence in which the number of 180° pulses increases in successive experiments to trace out the magnetization decay. However, this method suffers from the differential residual C−H dipolar couplings due to the varying evolution period and pulse imperfections due to the varying number of pulses. The present experiment avoids these problems by using a nearly constant evolution period and a constant number of π pulses with a highly compensated phase cycling scheme. The duration of the π-pulse train for $n = 4$ is at least $8\tau_r$ (for $\tau = 0$) and at most $10\tau_r$ (for $\tau = \tau_r$). The difference is sufficiently small that the signal decay is mostly unaffected by the different residual C−H dipolar coupling. Due to the slightly varying length of the π-pulse train, the τ-dependent decay curve is also slightly asymmetric with respect to the center of the rotor period.

The resolvable Cα signals in the 1D CSA-filter experiment are limited by the ratio of the Cα isotropic shift dispersion with the ^{13}C line width. Under our experimental conditions, the ^{13}C line widths range from 0.8 to 1.2 ppm. Therefore, about 30 $^{13}C\alpha$ resonances can be resolved. To extract more CSA parameters simultaneously, the 1D CSA-filter experiment needs to be extended to two dimensions. We use the ^{15}N chemical shift as a second dimension to reduce resonance overlap. The 2D $^{15}N-^{13}C$ correlation pulse sequence with a ^{13}C CSA-filter is shown in Figure 1b. The π-pulse train responsible for generating the magnetization decay is inserted after CP from ^1H to ^{13}C, and before the $^{13}C-^{15}N$ correlation sequence, which has been described previously.[30]

Results

Calculated CSA Decay Curves. Figure 2a shows the simulated CSA decay curves for $\Delta\sigma$ ranging from 15 to 40 ppm in steps of 1 ppm. This range covers the chemical shift anisotropies of most aliphatic carbons in amino acids. At small τ values ($\tau < \tau_r/4$), the time signals decrease monotonically with increasing $\Delta\sigma$, as expected from eq 6. For small values of $\Delta\sigma$, the decay is also monotonic with τ for the first half of the rotor period. As $\Delta\sigma$ increases, the decay curves exhibit increasing oscillatory features. At $\Delta\sigma = 40$ ppm, a prominent local maximum at $\tau = \tau_r/2$ is observed along with negative minima on both sides.

Since the current CSA-filter experiment records only the cosine component of the magnetization, the decay curves correspond to symmetrized chemical shift spectra after Fourier transformation. Thus, the sign of $\Delta\sigma$ is not obtained from the experiment. This could be changed by acquiring both the cosine and sine components of the magnetization, using an extended phase cycle for the 90° pulse before the z-filter. The tradeoff is the doubled signal-averaging time.

To examine the effect of the asymmetry parameter on the intensity decays, we show three sets of decay curves with $\Delta\sigma = 20$, 30, 40 ppm and $\eta = 0$, 0.4, 1 (Figure 2b). It can be seen that larger η values shift the intensities in the direction of smaller anisotropies. For example, the decay curve for ($\Delta\sigma = 20$ ppm, $\eta = 1$) resembles the ($\Delta\sigma = 18$ ppm, $\eta = 0$) curve (not shown). If the spectral sensitivity were limited, these two chemical shift tensors would not be easily distinguishable. An assumption of $\eta = 0$ can underestimate $\Delta\sigma$ while an assumption of $\eta = 1$ tends to overestimate $\Delta\sigma$. This uncertainty in $\Delta\sigma$ resulting from the uncertain η is about 10% for the chemical shift range examined here. Fortunately, as the CSA increases, η-induced line shape variations become more distinct from $\Delta\sigma$-induced changes.

(30) Hong, M.; Griffin, R. G. *J. Am. Chem. Soc.* **1998**, *120*, 7113−7114.

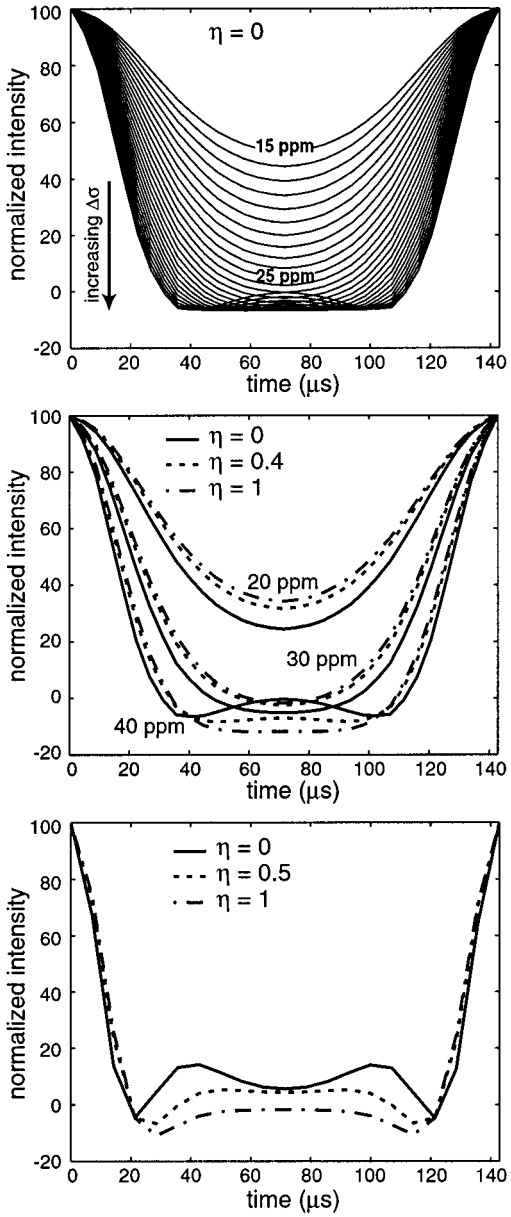

Figure 2. (a) Calculated CSA decay curves for $\Delta\sigma$ from 15 to 40 ppm in increments of 1 ppm and $\eta = 0$. (b) Calculated CSA decay curves for $\Delta\sigma = 20$, 30, and 40 ppm. For each anisotropy, $\eta = 0$ (solid lines), 0.4 (dashed lines), and 1 (dash−dotted lines) are calculated. The ^{13}C Larmor frequency is 75.5 MHz, and the spinning speed is 7 kHz. (c) Calculated CSA decay curves for $\Delta\sigma = 40$ ppm and $\eta = 0$ (solid line), 0.5 (dashed line), and 1 (dash−dotted line), at a ^{13}C Larmor frequency of 125 MHz and a spinning speed of 7 kHz.

Since the chemical shift interaction scales with the magnetic field, higher magnetic fields displace the onset of the oscillatory features toward smaller chemical shift anisotropies as expressed in ppm values. To demonstrate this, we calculated the CSA decay curves for $\Delta\sigma = 40$ ppm and $\eta = 0$, 0.5, 1, using a ^{13}C Larmor frequency of 125 MHz (Figure 2c). The $\eta = 0$ curve exhibits three local maxima in the rotor period. Larger asymmetry parameters damp the amplitude of the oscillation. The three curves are clearly distinguishable. Therefore, at larger magnetic fields, both the chemical shift anisotropy and the asymmetry parameter can be measured with higher accuracy.

Increased sensitivity to CSAs can also be achieved by extending the duration of the π-pulse train. According to eq 3, a larger n increases the dynamic phase Φ_{CSA} so that the decay envelope changes in a direction that corresponds to larger CSAs.

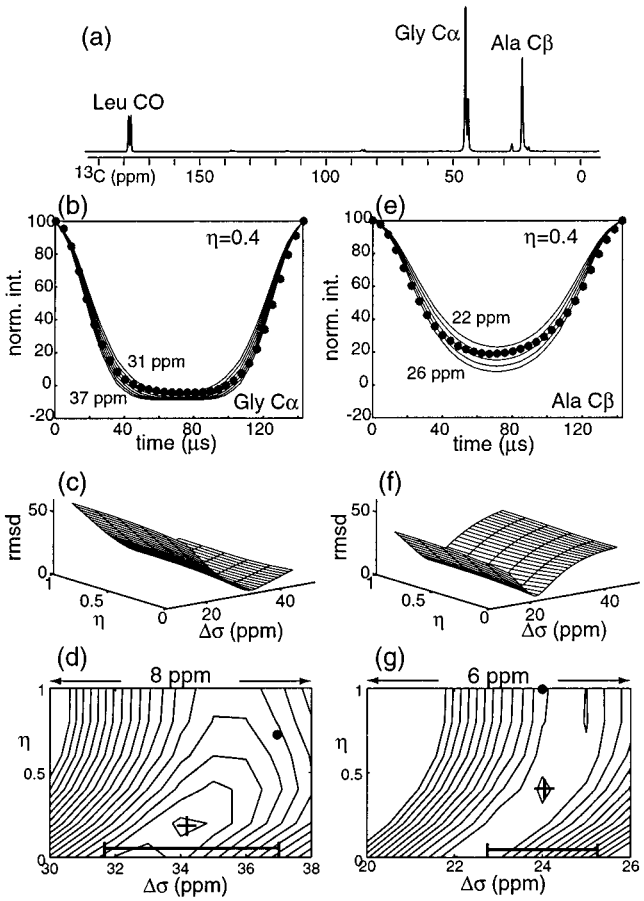

Figure 3. CSA decay curves of Gly Cα and Ala Cβ. (a) ^{13}C CPMAS spectrum of the amino acid mixture A/G/L. (b) Experimental CSA decays (circles) of [2-^{13}C]glycine and calculated curves for $\Delta\sigma$ from 31 to 37 ppm at $\eta = 0.4$. (c) The glycine rmsd between the experiment and the simulation as a function of the asymmetry parameter η and the anisotropy span $\Delta\sigma$. (d) Expanded region of the glycine rmsd plot. The best fit is indicated by a cross, and the literature value is shown as a circle. The horizontal bar indicates the uncertainty in $\Delta\sigma$. (e) Experimental CSA decays (circles) of [3-^{13}C]alanine and calculated curves from 22 to 26 ppm at $\eta = 0.4$. (f) The alanine rmsd as a function of η and $\Delta\sigma$. (g) Expanded region of the alanine rmsd plot.

In the frequency domain, this corresponds to reduced centerband intensity and increased sideband intensities. A similar amplification of the anisotropy has been demonstrated previously for the dipolar interaction.[31]

One-Dimensional Chemical Shift Anisotropy Filter. Figure 3 shows the experimental CSA decay curves for the amino acids glycine and alanine. The ^{13}C CPMAS spectrum of the mixture A/G/L (Figure 3a) exhibits strong signals from the three labeled carbons, Gly Cα, Ala Cβ, and Leu CO. The intensity differences result mostly from the different molar quantities of the three amino acids used in the mixture. A series of 32 ^{13}C spectra, corresponding to filter times $\tau_n = n\cdot\tau_r/32$ ($n = 0, 1, 2, ..., 31$), was acquired using the pulse sequence of Figure 1a. The peak intensities were normalized with respect to the $\tau = 0$ spectrum. They were plotted as a function of τ for Gly Cα (Figure 3b) and Ala Cβ (Figure 3e). The intensities at $\tau = \tau_r$ were taken to be identical with those at $\tau = 0$. Both decay curves exhibit a minimum at $\tau \approx \tau_r/2$, but with drastically different values. The Gly Cα signal decays to a negative value of −4.5%, while the Ala Cβ signal decays to +20%. This is qualitatively consistent with the larger anisotropy of the methylene carbon compared to the methyl carbon. Quantitatively, the CSA decay of glycine Cα falls between $\Delta\sigma$ of 31 and 37 ppm (assuming $\eta = 0.4$), while the $\Delta\sigma$ of Ala Cβ is bracketed by the 22- and 26-ppm simulations ($\eta = 0.4$).

To extract the chemical shift anisotropies quantitatively, we determined the minimum root-mean-square deviations between the calculated and the experimental intensities. Figure 3c and Figure 3f display the rmsd plots for Gly Cα and Ala Cβ, respectively, as a function of $\Delta\sigma$ and η. A $\Delta\sigma$ increment of 1 ppm and an η increment of 0.2 were used in the simulations. For Gly Cα, a valley of lowest rmsd values from ($\Delta\sigma$, η) of (32 ppm, 0) to (37 ppm, 0.75) is found. The density of the contour lines is low along the length of this valley (Figure 3d), indicating that high $\Delta\sigma$ values combined with high η give similarly good fits as low $\Delta\sigma$ values combined with low η. The global minimum rmsd occurs at $\Delta\sigma = 34$ ppm, which corresponds to the best fit. This result differs by 3 ppm from the literature value of 37 ppm.[32] The 8% error margin may be attributed to the fact that the Gly Cα has the strongest residual ^{13}C−^{1}H dipolar couplings among all amino acids, since it has two directly bonded protons.

The rmsd plot for Ala Cβ exhibits a similar valley of low rmsd values from (22.5 ppm, 0) to (25 ppm, 1). The global minimum occurs at (24 ppm, 0.4) (Figure 3g). This $\Delta\sigma$ agrees perfectly with the CSA obtained from the static spectrum of alanine.[32] If the literature asymmetry parameter $\eta = 1$ is used as an input, then a $\Delta\sigma$ of 25 ppm is obtained, a deviation of only 1 ppm.

The 1D CSA-filter experiment was also applied to selectively and extensively ^{13}C-labeled ubiquitin, whose ^{13}C CPMAS spectrum is shown in Figure 4a. More than 50 ^{13}Cα sites in ubiquitin are labeled by the [2-^{13}C]glycerol scheme. These resonate between 40 and 70 ppm, thus signal overlap is considerable. However, upfield between 10 and 20 ppm, the spectrum is less crowded. In particular, the resonance at 14 ppm results from several Ile Cδ1 sites according to the solution NMR chemical shifts. Since the end of the long isoleucine side chain should be minimally affected by the backbone conformation, these Cδ1 CSAs are expected to have a narrow dispersion. Indeed, the CSA decay curve of the Ile Cδ1 signal (Figure 4b) falls between the 18- and 22-ppm simulations. The 2D rmsd plot (Figure 4c) shows a narrow valley of low rmsd values from (19.5 ppm, 0) to (21.5 ppm, 1), with the global minimum at $\Delta\sigma = 20.5$ ppm (Figure 4d). This is in excellent agreement with the literature $\Delta\sigma$ of 21 ppm.[32] The low rmsd valley for this site is aligned more closely with the η axis than the previous two cases, indicating that the $\Delta\sigma$ determination is less sensitive to η.

The 2D rmsd analyses for these three carbon sites suggest that except for CH_2 groups, the uncertainty of the CSA determination is about ±1 ppm, at the magnetic field strength and spinning speed used here. This is an adequate error margin, since the conformation-dependent variations in the Cα CSAs should be much larger, according to both solution NMR measurement and the quantum mechanical calculations.

Chemical-Shift-Anisotropy-Filtered 2D ^{15}N−^{13}C Correlation. To determine the chemical shift anisotropy of multiple Cα sites simultaneously, resonance overlap must be minimized. This is partially achieved by 2D ^{15}N−^{13}C correlation. Figure 5 displays four 2D CSA-filter spectra of ^{13}C2-glycerol-labeled ubiquitin, acquired at τ values of 0, 36.7 ($\tau_r/4$), 54.7 ($3\tau_r/8$), and 72.4 μs ($\tau_r/2$). The assignment of some of the resolved

(31) Hong, M.; Gross, J. D.; Rienstra, C. M.; Griffin, R. G.; Kumashiro, K. K.; Schmidt-Rohr, K. *J. Magn. Reson.* **1997**, *129*, 85−92.
(32) Ye, C.; Fu, R.; Hu, J.; Hou, L.; Ding, S. *Magn. Reson. Chem.* **1993**, *31*, 699−704.

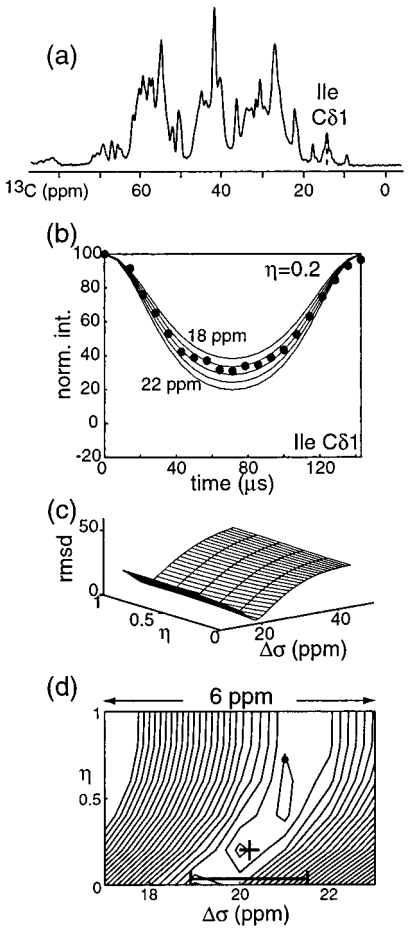

Figure 4. (a) ^{13}C CPMAS spectrum of [2-^{13}C] glycerol labeled ubiquitin. (b) Experimental CSA decays (circles) of $^{13}C\delta1$-isoleucine and calculated curves for $\Delta\sigma = 18$ to 22 ppm at $\eta = 0.2$. (c) The rmsd of isoleucine between the experiment and the simulation as a function of η and $\Delta\sigma$. (d) Expanded region of the isoleucine rmsd plot. The best fit (20.5 ppm) is indicated by a cross, and the literature value (21 ppm) is shown as a circle. The horizontal bar indicates the uncertainty in $\Delta\sigma$.

resonances is indicated.[33] These resonances are categorized as α-helical (bold), β-sheet (bold underline), and β-turn conformations (bold italics), based on the crystal structure of the protein.[27] Several types of amino acids occur in different secondary structures. These include Val-26 (helix) and Val-70 (sheet), Ile-30 (helix) and Ile-13 (sheet), Ser-57 (helix) and Ser-20 (turn), and Lys-29 (helix) and Lys-6 (sheet).

We first analyze the spectra qualitatively by identifying the resonances that survive the CSA filter. As τ increases from 0 to 36.7 μs, several β-sheet Cα signals decay first. This is true, for example, for the ^{15}N−$^{13}C\alpha$ resonances of Gln-40, Gln-41, and Phe-4 at 116−120 ppm in the ^{15}N dimension and about 55 ppm in the ^{13}C dimension (dashed circle). Another area where the intensities are reduced is (125−130 ppm, 60−62 ppm) for Val-70 and Ile-13. In contrast to the fast decaying β-sheet resonances, α-helical resonances such as Val-26 and a few β-turn resonances such as Thr-55 persist in the spectrum. As τ increases further, the spectrum becomes increasingly simple, since some of the initially unresolved signals have decayed. At the longest filter time of 72.4 μs, most of the remaining resonances can be assigned to the α-helical residues, with the exception of two β-turn signals, Ser-20 and Thr-55.

(33) Wang, A. C.; Grzesiek, S.; Tschudin, R.; Lodi, P. J.; Bax, A. *J. Biomol. NMR* **1995**, *5*, 376−382.

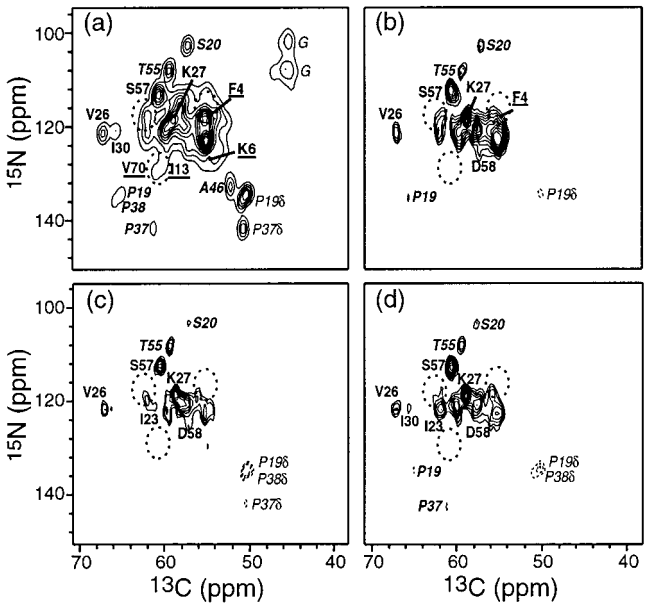

Figure 5. 2D ^{15}N−^{13}C spectra of ^{13}C,^{15}N-ubiquitin with variable delay times τ. (a) $\tau = 0$ μs, number of scans per t_1 slice (NS) = 64. (b) $\tau = 35.7$ μs, NS = 64. (c) $\tau = 57.1$ μs, NS = 128. (d) $\tau = 72.4$ μs, NS = 192. Spinning speed: 7 kHz. Assignment was made based on solution NMR.[33] The helical residues are indicated in bold, the sheet residues in bold underline, and the turn residues in bold italics. Dashed circles highlight regions of drastic intensity decays with longer filter time τ. Total signal averaging time: 21 h.

Therefore, the main observation from these 2D CSA-filter spectra is that the Cα signals of helical residues survive longer than those of the sheet residues. This indicates that helical Cα CSAs are smaller than the sheet Cα CSAs. This difference is manifested more clearly by superimposing the experimental spectra at $\tau = 0$ and 72.4 μs with two sets of peak positions obtained from solution NMR (Figure 6). In the first subset, all labeled $^{13}C\alpha$ sites, regardless of their conformation, are included. Leucines are the only excluded residues, since their Cα sites are not labeled by [2-^{13}C]glycerol (Figure 6a). In the second subset, only the helical Cα sites are plotted. A remarkable correlation is immediately discernible: while the $\tau = 0$ experimental spectrum expectedly matched the set with nearly all peaks, the $\tau = 72.4$ μs spectrum matched closely the pattern of the helical residues. Particularly prominent are the Cα sites of Ile-23, Val-26, Lys-27, and Ile-30. In fact, all helical residues except for Lys-33, Glu-34, and Tyr-59 have matching experimental intensities. Interestingly, the three exceptional residues are all located at the ends of the two helices in ubiquitin. Thus, their above-average anisotropies may result from a "helix end" effect, where the conformation-based reduction of the CSA is weaker at the termini than in the central portion of the helices.

Several types of nonhelical resonances in the 2D spectra merit additional comments. First, two β-turn resonances, Thr-55 and Ser-20, clearly remain in all spectra. The basis for their small CSAs is not understood. It is interesting that both sites exhibit unusually upfield ^{15}N chemical shifts, suggesting that other special conformational or packing factors may contribute to the chemical shifts of the backbone atoms in these two residues. Second, the Pro-19 and Pro-37 Cα resonances exhibit negative intensities at $\tau = 36.7$ μs, become undetectable at the intermediate time of $3\tau_r/8$, and reappear negative at $\tau_r/2$. These significant intensity oscillations are consistent with the large, 37-ppm, anisotropy measured from the static spectra of the amino acid proline.[32] In comparison, the glycine Cα signals decay and never oscillate back. This is the signature of a large anisotropy and a

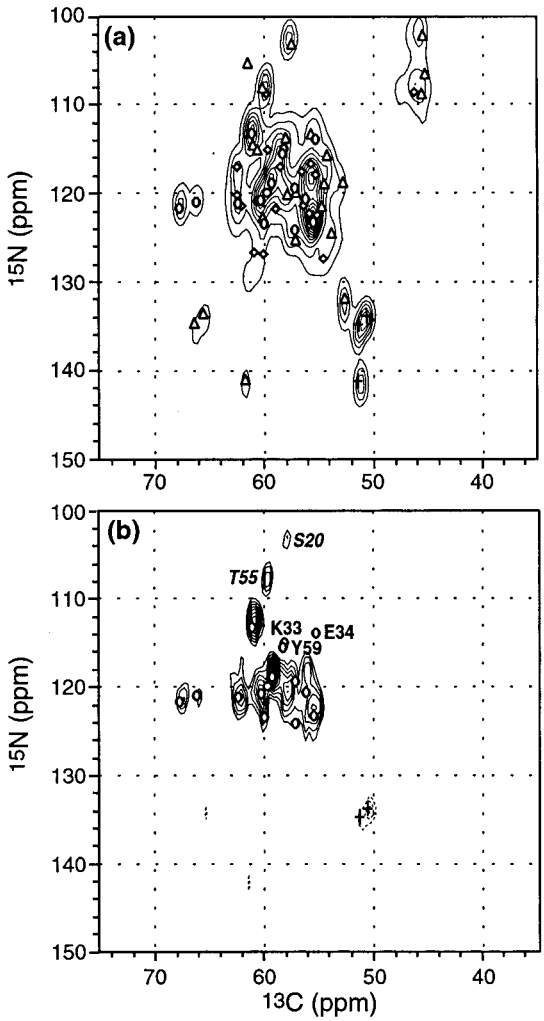

Figure 6. Simulated (symbols) and experimental (contours) 2D CSA spectra of ^{13}C2-ubiquitin for correlating Cα CSA with the secondary structure. (a) Resonances of all residues labeled by the [2-^{13}C]glycerol scheme. Solution NMR chemical shifts are used to simulate the ^{15}N−^{13}C spectra. Circles: helical residues. Triangles: turn residues. Diamonds: sheet residues. Crosses: Pro Cδ. The experimental spectrum corresponds to $\tau = 0$ μs. (b) Resonances of all helical residues. The experimental spectrum corresponds to $\tau = 72.4$ μs.

larger η. Finally, we observe negative intensities for the proline Cδ resonances in all but the initial spectra. The proline Cδ has the largest chemical shift anisotropy among all amino acids, about 60 ppm according to static powder spectra[32] and with an asymmetry parameter of about 0.5. The corresponding decay curve is similar to those shown in Figure 2c, where the intensities decay rapidly to below 0 and remain there for most of the rotor period.

Discussion

Diagnosis of Protein Secondary Structure by the Solid-State CSA Filter. Determination of the backbone conformation is the necessary first step toward the elucidation of the complete three-dimensional structure of proteins. The correlation between the ^{13}Cα chemical shift anisotropy and the backbone conformation provides a potentially efficient probe of the secondary structure of insoluble and noncrystallizable proteins. Until now, knowledge of the protein CSAs has been relatively scarce, since solid-state NMR has been unable to measure many CSAs simultaneously on isotopically labeled proteins. The present CSA-filter technique in combination with biosynthetic selective and extensive ^{13}C labeling solves this problem. The experiment gives direct evidence that helical residues have smaller Cα CSAs than sheet residues, without assuming the orientation or the asymmetry parameter of the chemical shift tensor. In the 2D CSA-filtered ^{15}N−^{13}C spectra, the helical residues correspond to most of the remaining resonances while the sheet residues are filtered. Therefore, the 2D CSA-filter experiment provides a simple and robust tool for determining the secondary structure of proteins qualitatively.

To obtain conformational information from the CSA-filter experiment, the NMR spectra need to be assigned. In this study, we used the solution NMR chemical shifts of ubiquitin to facilitate the verification of the CSA-structure correlation. However, knowledge of solution NMR assignment is generally not available for the insoluble proteins to which this CSA-filter technique is particularly relevant. For such insoluble proteins, there are now a number of multidimensional solid-state NMR assignment techniques, such as 2D N(CO)CA, 3D NCACB, time-dependent 2D ^{15}N−^{13}C correlation, and 2D ^{13}C−^{13}C correlation.[25,26] In fact, some information on amino acid type assignment is already contained in the ^{15}N−^{13}C 2D CSA-filter spectrum at $\tau = 0$. Aided by these resonance assignment experiments, the 2D CSA-filter technique should be useful for identifying α-helical residues in solid proteins.

Comparison of Solid-State, Solution, and Calculated Cα CSAs. The solution NMR dipolar-CSA cross-correlated relaxation experiment[15] found Cα CSAs of 6.1 ± 4.9 ppm for helical residues and 27.1 ± 4.3 ppm for sheet residues. Quantum mechanical calculations predicted the same trend of larger tensor spans for sheet over helical residues. However, the CSA gap according to the latter study is much smaller.[16] The average helical CSA was calculated to be 22 ppm while the average sheet CSA was 34 ppm. In other words, the calculated helical CSAs are more than 10 ppm larger than the solution NMR CSAs. In addition, the quantum mechanical calculations predicted that the shielding surfaces depend not only on (ϕ, ψ) but also on the side chain torsion angles χ_1 and χ_2.

The present solid-state CSA-filter experiment sheds light on the origin of the different helical CSAs between the solution NMR measurement and the quantum chemical calculations. The comparison among the experimental solid-state CSAs, the solution NMR results, and the ab initio calculations is shown in Figure 7. The intensities of a number of relatively resolved resonances from the CSA-filter spectra are plotted. These include three helical resonances (Figures 7a and 7c) and four sheet resonances (Figures 7b and 7d). Among the helical resonances, Val-26 Cα is resolved in both the 1D and 2D spectra. Both decay curves are plotted to gauge the consistency between the 1D and the 2D experiments. A similar consistency check for the CSA decays of the sheet residues is provided by Ala-46 Cα, which is actually located in a type-III′ β-turn but exhibits a large CSA. The uncertainties of the experimental intensities vary from 1.5% to 7%, since the noise level of each spectrum is scaled by different amounts according to the initial peak intensities. For simplicity, these error margins are not indicated in Figure 7.

Superimposed with the experimental intensities are the calculated decay curves for the solution NMR and the quantum mechanical Cα CSAs. The solution NMR CSA decays (Figures 7a and 7b) were simulated with an asymmetry parameter of 0, which had been used in the analysis of the relaxation data. We calculated three decay curves for each backbone conformation, representing the lower limit, the average, and the upper limit

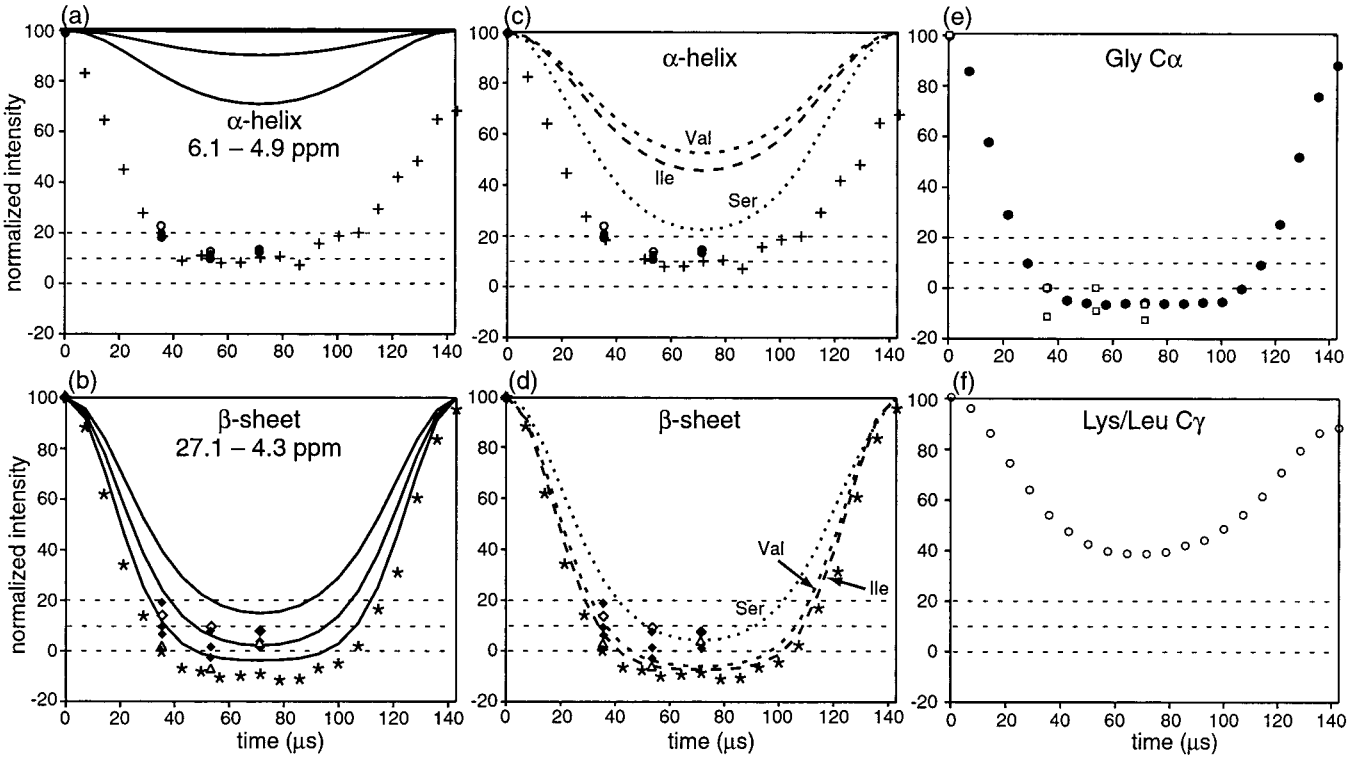

Figure 7. Comparison of conformation dependent Cα CSAs from solid-state NMR, solution NMR, and quantum mechanical calculations. (a) Solid curves: simulated solution NMR Cα CSAs for helical residues, 6.1 ± 4.9 ppm. Filled circles: 2D Cα intensities of helical resonances Ser-57, Lys-29, and Lys-27. Open circles: 2D Cα intensities of Val-26. Crosses: Cα intensities of Val-26 from 1D. Uncertainties are 1.2−6.7%. Thin dashed lines at 0%, 10%, and 20% normalized intensities guide the eye for comparison with the sheet CSAs. (b) Solid curves: simulated solution NMR Cα CSAs for sheet residues, 27.1 ± 4.3 ppm. Filled diamonds: 2D Cα intensities of sheet resonances Phe-4, Val-17, and Ile-61. Uncertainties are 1.0−7.7%. Open diamonds: 2D Cα intensities of Lys-6, with uncertainties of 4.0−8.7%. Triangles: Ala-46 from the 2D CSA filter. Stars: Ala-46 from the 1D CSA filter. (c) Ab initio helical Cα CSAs for Val (16.5 ppm, short-dashed line), Ile (18 ppm, long-dashed line), and Ser (24 ppm, dotted line). Experimental data points are the same as in (a). (d) Ab initio β-sheet CSAs for Val (−35 ppm), Ile (−37 ppm), and Ser (−29 ppm). Simulations are the same as in (c). Experimental data points are the same as in (b). (e) Experimental Cα CSAs of glycine. Squares: 2D intensities of two glycine resonances. Filled circles: 1D intensities. (f) Experimental Cγ CSAs of Lys and Leu from the 1D CSA filter.

of the measured CSAs. It can be seen clearly that the helical CSAs from the solid-state NMR experiments are larger than the solution NMR values well beyond the uncertainties of either measurement. At $\tau_r/2$, the intensity gap between the largest solution NMR CSA (the lowest solid curve) and the smallest solid-state NMR CSA (the highest experimental point) is more than 55%, relative to the initial intensity of 100%. In comparison, better agreement for the β-sheet CSAs is found between the solid-state and the solution NMR results (Figure 7b).

The decay curves corresponding to the ab initio Cα CSAs of Val, Ile, and Ser in helical and sheet residues are displayed in Figures 7c and 7d. For each residue type, the CSAs calculated for the major χ_1 conformers were averaged.[16] The resulting valine helical and sheet Cα CSAs are 16.5 and 35 ppm, respectively. The isoleucine helical and sheet CSAs are 18 and 37 ppm, respectively. For serine, the corresponding values are 24 and 29 ppm. The figures show that the quantum mechanical helical Cα CSAs are much closer to the solid-state NMR results than the solution NMR experiments are, although the ab initio anisotropies are still somewhat smaller than the results of the CSA-filter measurements. For the sheet conformation, the calculated range of CSAs agrees quite well with the experimental intensities.

The different CSAs between the solution-NMR measurement and the quantum chemical calculation can be attributed to the fact that different chemical shift quantities are addressed in the two approaches. The relaxation interference experiment measures the projection of an axially symmetric chemical shift tensor onto the dipolar bond vector.[34−37] Specifically, $\Delta\sigma^* = \sigma_{par} - \sigma_{orth}$, in which the parallel and orthogonal tensor elements are defined with respect to the Cα−Hα bond, is measured. Deviation of the tensor orientation from the Cα−Hα bond is accounted for by the second Legendre polynomial, $P_2(\cos\theta) = (3\cos^2\theta - 1)/2$, where θ is the angle between the Cα−Hα bond and the most deshielded element σ_{11} of the chemical shift tensor. Therefore, the CSA-dipolar cross correlation experiment does not separate the effects of the tensor orientation from the tensor magnitude. This contrasts with the ab initio calculations and the present solid-state NMR experiment, which determine the shielding tensor breadth independent of an internuclear vector.

In fact, the orientation of the Cα shielding tensor may deviate significantly from the Cα−Hα bond. Quantum mechanical calculations predicted that the angle between the Cα−Hα bond and the most deshielded element σ_{11} of the Cα shielding tensor vary from $\theta = 8°$ in sheet residues to $\theta = 82°$ in helical residues.[16] If this is the unique axis in both the helical and sheet residues, then the relaxation interference experiment actually measures $\Delta\sigma^* \cdot P_2(\cos 82°) \approx -0.5 \cdot \Delta\sigma^*$ for the helical residues

(34) Damburg, P.; Jarvet, J.; Allard, P.; Graslund, A. *J. Biomol. NMR* **1999**, *15*, 27−37.
(35) Fushman, D.; Cowburn, D. *J. Am. Chem. Soc.* **1998**, *120*, 7109−7110.
(36) Tessari, M.; Vis, H.; Boelens, R.; Kaptein, R.; Vuister, G. W. *J. Am. Chem. Soc.* **1997**, *119*, 8985−8990.
(37) Tjandra, N.; Szabo, A.; Bax, A. *J. Am. Chem. Soc.* **1996**, *118*, 6986−6991.

but $\Delta\sigma^* \cdot P_2(\cos 8°) \approx \Delta\sigma^*$ for the sheet residues. This could account for the small helical CSAs obtained from the solution NMR experiment. On the basis of this analysis, the actual helical CSAs should be 12.2 ± 9.8 ppm, the upper bound of which is much closer to the solid-state CSA results for the helical residues.

A second complicating factor that contributes to the different helical CSAs determined by the three methods is the asymmetry parameter of the Cα shielding tensor. Static NMR experiments on powder samples of single amino acids[32] and ab initio calculations indicate that the asymmetry parameter of the Cα tensor covers the full range of 0 to 1. Thus, the assumption of axial symmetry in the analysis of the solution relaxation data is likely to have a nonnegligible effect on the determination of $\Delta\sigma$. The relaxation interference between an asymmetric chemical shift tensor and a dipolar vector has been analyzed previously[38] by the decomposition of the asymmetric tensor into the sum of two axially symmetric tensors with a certain relative orientation. It is possible that the single-tensor assumption with $\eta = 0$ in the solution NMR experiment effectively amounts to removing the contribution of the second tensor, thus underestimating the real anisotropy.

Nevertheless, for the purpose of determining protein secondary structure, the CSA-dipole relaxation interference experiment is quite effective. If the change in Cα tensor orientation between the helical and sheet residues proves to be true experimentally, then the lack of distinction between the magnitude and the orientation actually constitutes an advantage to the solution NMR technique.

Glycine Cα and Leu and Lys Side Chain Carbon CSAs. In addition to the helical and sheet Cα sites, we also examined the CSAs of several other carbons. These include the CH_2 group of two glycine residues (Figure 7e) and the Cγ signals of several Lys and Leu residues at isotropic chemical shifts of about 27 ppm (Figure 7f). The Gly Cα signals give an upper bound to all the CSAs measured here, while the side chain Cγ signal provides a lower bound. The relatively slow CSA decay of the Cγ signal verifies that the large decays observed for the ^{13}Cα of helical and sheet residues are indeed conformational effects and not experimental artifacts. This is demonstrated by five representative 1D CSA-filter spectra with variable delays τ (Figure 8). All five spectra show consistently high intensities of the side chain Cγ signal.

Advantages of the CSA Filter Technique. The main advantages of the CSA-filter technique are its insensitivity to experimental artifacts and its ease of implementation under standard MAS conditions. The number of 180° pulses remains constant in the experiment. There is no "collision" of pulses, and the total duration of the pulse train is nearly constant. The experiment does not require special probeheads such as slow-spinning MAS probes[18,19] or switching-angle-spinning probes.[20−22] It can be applied under medium to high spinning speeds to achieve high resolution, since only two π pulses are applied in each rotor period. As the magnetic field strength increases, the experiment will exhibit higher $\Delta\sigma$ accuracy. The experiment does not sacrifice signal sensitivity, which is a limitation of the principal-value spectroscopy.[39] The same 2D ^{15}N−^{13}C correlation experiment at $\tau = 0$ is useful for resonance assignment in the solid state, thus reducing the need for solution NMR chemical shifts. Most importantly, when combined with extensive isotopic labeling,[7,40] this CSA-filter experiment can provide backbone conformational constraints for multiple residues simultaneously. This is useful for structure refinement of proteins when used in conjunction with torsion-angle experiments. Moreover, it should be useful for generating a larger empirical basis for the correlation of CSA and structure in proteins.

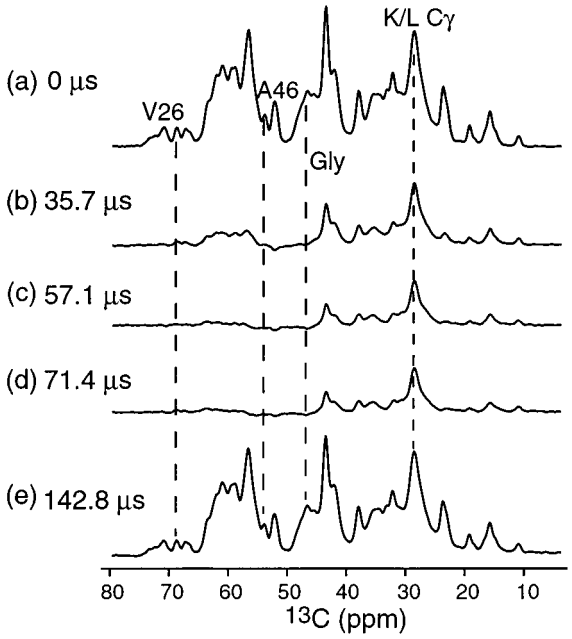

Figure 8. 1D CSA filter spectra of ubiquitin for $\tau = 0$ (a), 35.7 (b), 57.1 (c), 71.4 (d), and 142.8 (e) μs. Spinning speed: 7 kHz.

Conclusions

A technique for measuring the chemical shift anisotropies of multiple sites in extensively isotopically labeled proteins is presented and demonstrated on ubiquitin. The chemical shift anisotropy is reintroduced under magic-angle spinning by a train of 180° pulses in which the second half of the pulse train is displaced with respect to the first half. It is shown that the ^{13}C CSAs can be measured with the accuracy of ±1 ppm for CH_3 groups and CH groups, and of ± 3 ppm for CH_2 groups. For extensively isotopically labeled proteins, the technique can be combined with ^{15}N−^{13}C 2D correlation to enhance the site resolution. The 2D CSA-filter spectrum at a delay of half a rotor period corresponds predominantly to α-helical residues. This confirms the previous finding that helical residues have smaller Cα CSAs than sheet residues. However, the helical CSAs obtained from the solid-state experiment are significantly larger than the values estimated by solution NMR and agree better with the quantum mechanical calculations. The difference in the helical CSAs between solution and solid-state NMR may be attributed to the different assumptions of the shielding tensor orientation and asymmetry parameter. This CSA-filter experiment promises to be a useful diagnostic tool for the secondary structure of proteins. It is also a general method for determining the chemical shift anisotropies of other complex disordered solids.

Acknowledgment. M. Hong thanks S. Su for helping with the analysis of the CSA data and K. Saalwächter for insightful discussions. The author is grateful to the National Science Foundation for a POWRE grant that funded this work and partial support by the National Science Foundation Materials Research Science and Engineering Center at the University of Massachusetts.

JA994119N

(38) Goldman, M. *J. Magn. Reson.* **1984**, *60*, 437−452.
(39) deSwiet, T. M. *J. Chem. Phys.* **1999**, *110*, 5231−5237.
(40) Hong, M.; Jakes, K. *J. Biomol. NMR* **1999**, *14*, 71−74.